NASA TN D-354

TECHNICAL NOTE

D-354

EFFECTS OF STING-SUPPORT DIAMETER ON THE BASE

PRESSURES OF AN ELLIPTIC CONE AT MACH

NUMBERS FROM 0.60 TO 1.40

By Louis S. Stivers, Jr., and Lionel L. Levy, Jr.

Ames Research Center
Moffett Field, Calif.

NATIONAL AERONAUTICS AND SPACE ADMINISTRATION

WASHINGTON   February 1961

NATIONAL AERONAUTICS AND SPACE ADMINISTRATION

TECHNICAL NOTE D-354

EFFECTS OF STING-SUPPORT DIAMETER ON THE BASE

PRESSURES OF AN ELLIPTIC CONE AT MACH

NUMBERS FROM 0.60 TO 1.40

By Louis S. Stivers, Jr., and Lionel L. Levy, Jr.

SUMMARY

Measurements were made to determine the effects of sting-support diameter on the base pressures of an elliptic cone with ratio of cross-section thickness to width of 1/3 and a plan-form semiapex angle of 15°. The investigation was made for model angles of attack from -2° to +20°, at Mach numbers from 0.60 to 1.40, and for a constant Reynolds number of 1.4 million, based on the length of the model.

The results indicated that the sting interference decreased the base axial-force coefficients by substantial amounts up to a maximum of about one-third the value of the coefficient for no sting interference. There was no practical diameter of the sting for which the effects of the sting on the base pressures would be negligible throughout the Mach number and angle-of-attack ranges of the investigation.

INTRODUCTION

Many of the recent configurations contemplated for atmosphere re-entry vehicles are characterized in part by large, blunt, noncircular bases. During wind-tunnel tests of such a configuration, the model is usually mounted on a sting support attached to the large base. To evaluate the aerodynamic characteristics of the model accurately at subsonic and supersonic Mach numbers, the influence of the sting support on the base pressures must be known, particularly since the axial-force contribution of the base will be a large part of the total axial force on the model. Presently available data pertaining to sting interference on base pressures at subsonic and supersonic Mach numbers, such as given in references 1 to 8, were obtained for bodies of revolution with cylindrical, boattailed, or flared afterbodies. Such data cannot be expected to be generally applicable to bodies with large, noncircular bases.

It is the purpose of this paper to provide information on sting interference for an elliptic cone at Mach numbers ranging from 0.60 to 1.40 and angles of attack from -2° to +20°. The interference was determined from pressure measurements at several points on the base of the model.

NOTATION

B area of model base, 4.712 sq in.

C_{A_b} base axial-force coefficient (positive rearward), $\dfrac{\text{base axial force}}{q_\infty B}$

ΔC_{A_b} increment in base axial-force coefficient due to the sting, $\left(C_{A_b}\right)_{\text{with sting}} - \left(C_{A_b}\right)_{\text{without sting}}$

C_{P_b} base-pressure coefficient, $\dfrac{p_b - p_\infty}{q_\infty}$

d sting diameter

M free-stream Mach number

p_b static pressure on model base

p_∞ free-stream static pressure

q_∞ free-stream dynamic pressure

t thickness or minor axis of ellipse at model base (see fig. 1)

α angle of attack of model, deg

APPARATUS AND MODEL

Wind Tunnel

The investigation was conducted in the Ames 2- by 2-Foot Transonic Wind Tunnel. This tunnel utilizes a flexible nozzle and porous test-section walls to permit continuous operation up to a Mach number of 1.4, and to provide choke-free flow in the test section throughout the transonic Mach number range. A constant Reynolds number is maintained throughout the operational range of Mach numbers by controlling the stagnation pressure within the tunnel.

Model and Sting Support

The elliptic cone model had a ratio of cross-section thickness to width of 1/3, and a plan-form semiapex angle of 15°. Support for the model during the tests was provided by a fixed half-sting which was fitted on the right-hand side (facing upstream) of a reflection plate (see fig. 1(a)). This half-sting support extended about 10 diameters from the model base to a whole sting flare. On the left side of the reflection plate, any one of several "dummy" half-sting configurations was mounted for the investigation.

Five different half-sting configurations were used. These are illustrated in figure 1(b). Four removable half-stings provided a variation of the ratio of sting diameter to model base thickness from 0.619 to 0 and the fifth provided a change in the angle of the flare fairing used in the absence of a half-sting.

The sting length and flare angle for the model support were selected in an effort to eliminate the necessity of considering these items in the present evaluation of sting-support interference. The choice was made by using as a guide the critical length and flare angle data of reference 7. Although the data of this reference are not strictly applicable to the present model, it is believed that the appropriate criteria would not be more stringent for the present model.

Boundary-layer transition wires with a diameter of 0.006 inch were secured to the model surface with clear lacquer. One wire was placed around the model at a longitudinal station 0.56 inch from the apex. Between this station and the model base, additional wires were positioned on the upper and lower surfaces along rays which were located at a distance of 45 percent of the local span on each side of the model plane of symmetry. (See fig. 1(a).)

Orifices for measuring pressures on the base of the model at four points on each side of the reflection plate were located at the positions indicated in figure 1(c). The pressure leads were connected to pressure transducers located outside the tunnel.

TESTS

Two series of tests were made. A preliminary series was made to select a suitable reflection plate, and a final series of tests was made, using the selected plate illustrated in figure 1(a), to determine the effects of the various sting configurations on the base pressures on the model. The criteria for selecting the reflection plate were that it be of sufficient length and height to essentially isolate the pressure disturbances on each half of the model base, and that it not affect the

base pressures to a measurable degree. For the preliminary series, tests
were made with various sized plates and without a plate using only sting
configurations A and E (see fig. 1(b)). For both series of tests,
pressures were measured with the transition wires mounted on the model.
The visualization technique described in reference 9 was used to ascertain
that the wires were effective in producing a turbulent boundary layer.
In both series of tests, base pressures were measured at Mach numbers
ranging from 0.60 to 1.40 and at a Reynolds number of 1.4 million based
on the model length. The preliminary tests were limited to a few repre-
sentative Mach numbers and angles of attack, and to an angle-of-attack
range from 0° to 16°. The angle-of-attack range of the final tests was
from -2^O to $+20^O$.

CORRECTIONS AND PRECISION

No wall-interference corrections have been applied to the measured
base pressures of this report. Any existing wall effects are believed
to have been unaffected by sting configuration so that the data based
on differences in pressures due to the various changes in sting config-
uration are considered to be interference free.

Other factors which could have influenced the measured data have
been found to be insignificant and have been neglected. In addition to
any systematic errors that might be introduced by corrections which have
been neglected, the test data are subject to random errors of measurement
which influence the reliability of the data. The mean square errors or
standard deviations in Reynolds number, Mach number, angle of attack,
and pressure coefficient (or base axial-force coefficient) have been
evaluated by the method of reference 10. Representative values are
given in the following table:

Standard deviations			
Item	M = 0.60	M = 1.00	M = 1.40
R	$\pm 0.02 \times 10^6$	$\pm 0.02 \times 10^5$	$\pm 0.02 \times 10^6$
M	± 0.002	± 0.003	± 0.005
α	$\pm 0.02^O$	$\pm 0.02^O$	$\pm 0.02^O$
C_p (or C_A)	± 0.006	± 0.005	± 0.004

RESULTS AND DISCUSSION

The results of the investigation are presented in three forms; as base-pressure coefficients in figure 2, as base axial-force coefficients in figure 3, and as increments of base axial-force coefficient due to sting-diameter interference in figures 4 and 5. The pressure coefficients are presented for both halves of the model base, but for only six representative angles of attack. The base axial-force coefficients associated with the various removable half-sting diameters were determined as the negative of the average values of the base-pressure coefficients for the removable sting side of the reflection plate. The values for a sting diameter of zero were determined from an average of the values for sting configurations D and E. The increments of base axial-force coefficient are the changes in the coefficient from the values associated with no sting (zero sting diameter) to those corresponding to each diameter.

Before consideration is given to the effects of the sting support, a few significant characteristics of the base-pressure and base axial-force coefficients (figs. 2 and 3) should be noted. The pressure coefficients for each configuration are approximately uniform over each half of the model base. As was expected, however, the magnitude of the pressure coefficients on the removable-sting side of the reflection plate and the magnitude of the base axial-force coefficients varied significantly as the sting configuration was changed. On the fixed sting side of the plate the pressure coefficients remained essentially constant. A region of anomalous data for the removable-sting side of the plate exists at an angle of attack of 10° for Mach numbers near 0.95 (see figs. 2 and 3). In this region there were small or essentially no effects on the base pressures or base axial forces resulting from the changes in sting configuration. No explanation can be given for this irregularity.

The presence of the sting support generally caused substantial reductions in the base axial-force coefficients. The maximum reduction amounted to about -0.2, which was approximately one-third of the corresponding base axial-force coefficient for zero sting diameter. The largest effects of the sting at each angle of attack occurred at Mach numbers between 1.0 and 1.1 (see figs. 4 and 5). The increments of base axial-force coefficient due to the sting do not vary linearly with ratio of sting diameter to base thickness (fig. 4), and are not reduced significantly at supersonic Mach numbers until the ratio has been reduced to small values. Actually, there does not appear to be any practical value of the ratio that will provide negligible influence of the sting on the base axial-force coefficients throughout the range of Mach numbers from 0.60 to 1.40.

CONCLUSIONS

The results of the investigation of sting-support diameter effects on the base pressures of an elliptic cone at Mach numbers from 0.60 to 1.40 and for angles of attack from -2° to +20°, with Reynolds number held constant at 1.4 million, indicate the following:

1. The presence of the sting generally reduced the base axial-force coefficient by appreciable amounts. The maximum reduction diminished the base axial-force coefficient by about one-third.

2. There was no usable diameter of the sting for which the interference on the base pressures would be negligible throughout the ranges of Mach numbers and angles of attack of the tests.

Ames Research Center
    National Aeronautics and Space Administration
        Moffett Field, Calif., Oct. 19, 1960

REFERENCES

1. Perkins, Edward W: Experimental Investigation of the Effects of Support Interference on the Drag of Bodies of Revolution at a Mach Number of 1.5. NACA TN 2292, 1951.

2. Chapman, Dean R.: An Analysis of Base Pressure at Supersonic Velocities and Comparison with Experiment. NACA Rep. 1051, 1951.

3. Hart, Roger G.: Effects of Stabilizing Fins and a Rear-Support Sting on the Base Pressures of a Body of Revolution in Free Flight at Mach Numbers From 0.7 to 1.3. NACA RM L52E06, 1952.

4. Tunnell, Phillips J.: An Investigation of Sting-Support Interference on Base Pressure and Forebody Chord Force at Mach Numbers From 0.60 to 1.30. NACA RM A54K16A, 1955.

5. Donaldson, I. S.: The Effect of Sting Supports on the Base Pressure of a Blunt-Based Body in a Supersonic Stream. The Aeronautical Quarterly (British), vol. VI, pt. 3, Aug. 1955, pp. 221-229.

6. Cahn, Maurice S.: An Experimental Investigation of Sting-Support Effects on Drag and a Comparison with Jet Effects at Transonic Speeds. NACA Rep. 1353, 1958.

7. Lee, George, and Summers, James L.: Effects of Sting-Support Interference on the Drag of an Ogive-Cylinder Body With and Without a Boattail at 0.6 to 1.4 Mach Number. NACA RM A57I09, 1957.

8. Reese, David E., Jr., and Wehrend, William R., Jr.: Effects of Sting-Support Interference on the Base Pressures of a Model Having a Blunt-Nosed Cylinder Body and a Conical Flare at Mach Numbers of 0.65 to 2.20. NASA TM X-161, 1960.

9. Main-Smith, J. D.: Chemical Solids as Diffusible Coating Films for Visual Indications of Boundary-Layer Transition in Air and Water. British A.R.C. R. & M. No. 2755, 1954.

10. Beers, Yardley: Introduction to the Theory of Error. Addison-Wesley Pub. Co., Cambridge, Mass., 1953.

A
4
3
2

8

A
4
3
2

All dimensions in inches,
except as noted

Section A - A

Fixed half-sting,
.438 R

Removable
half-sting,
.438 R

Transition wires

Sting flare

4.7°

.875

.050

Reflection plate

1.909

.010

Transition wires

15°

.135

.56

4.242

7.917

A
4
3
2

Sting

t = 1.414

7

8.533

A

A

Model

Transition wires

5.937

1.980

4° bevel on edges,
both sides
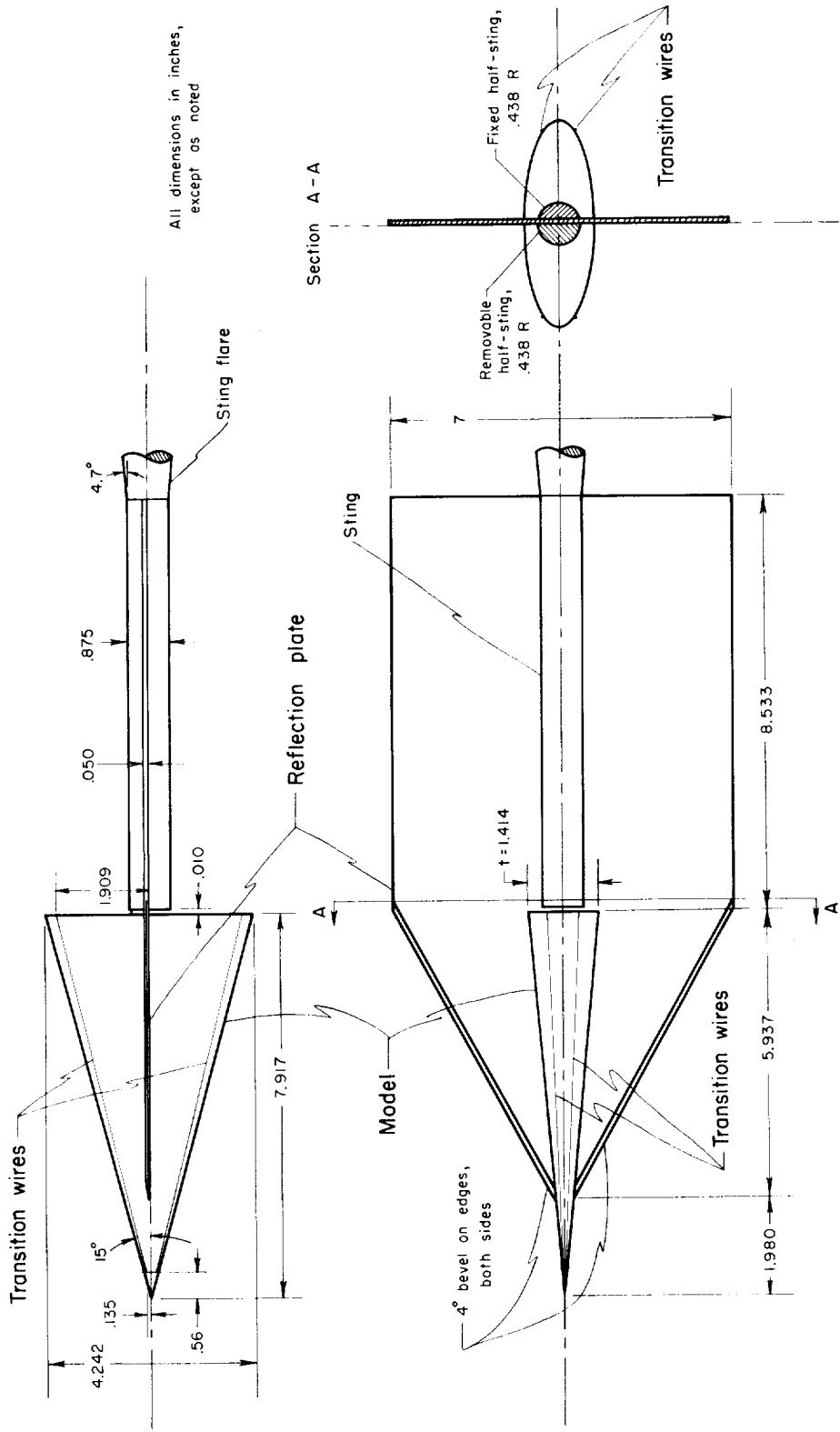
(a) Model, reflection plate, and sting configuration A.

Figure 1.- Geometrical information for the model and accessories.

Reflection plate

Model

Section A-A

8.533   4.7°

Fixed, .438 R

.010

8.523

Removable, .438 R

.875

$d/_t = .619$

Configuration A

Section A-A

8.533

Fixed, .438 R

6.743   4.7°

Removable, .292 R

$d/_t = .413$

Configuration B

Section A-A

8.533

Fixed, .438 R

4.958   4.7°

Removable, .146 R

$d/_t = .207$

Configuration C

Section A-A

8.533

Fixed, .438 R

3.183   4.7°

$d/_t = 0$

Configuration D

Section A-A

8.533

Fixed, .438 R

6.062   10°

$d/_t = 0$

Configuration E

All dimensions in inches
except as noted

(b) Description of sting configurations.

Figure 1.- Continued.
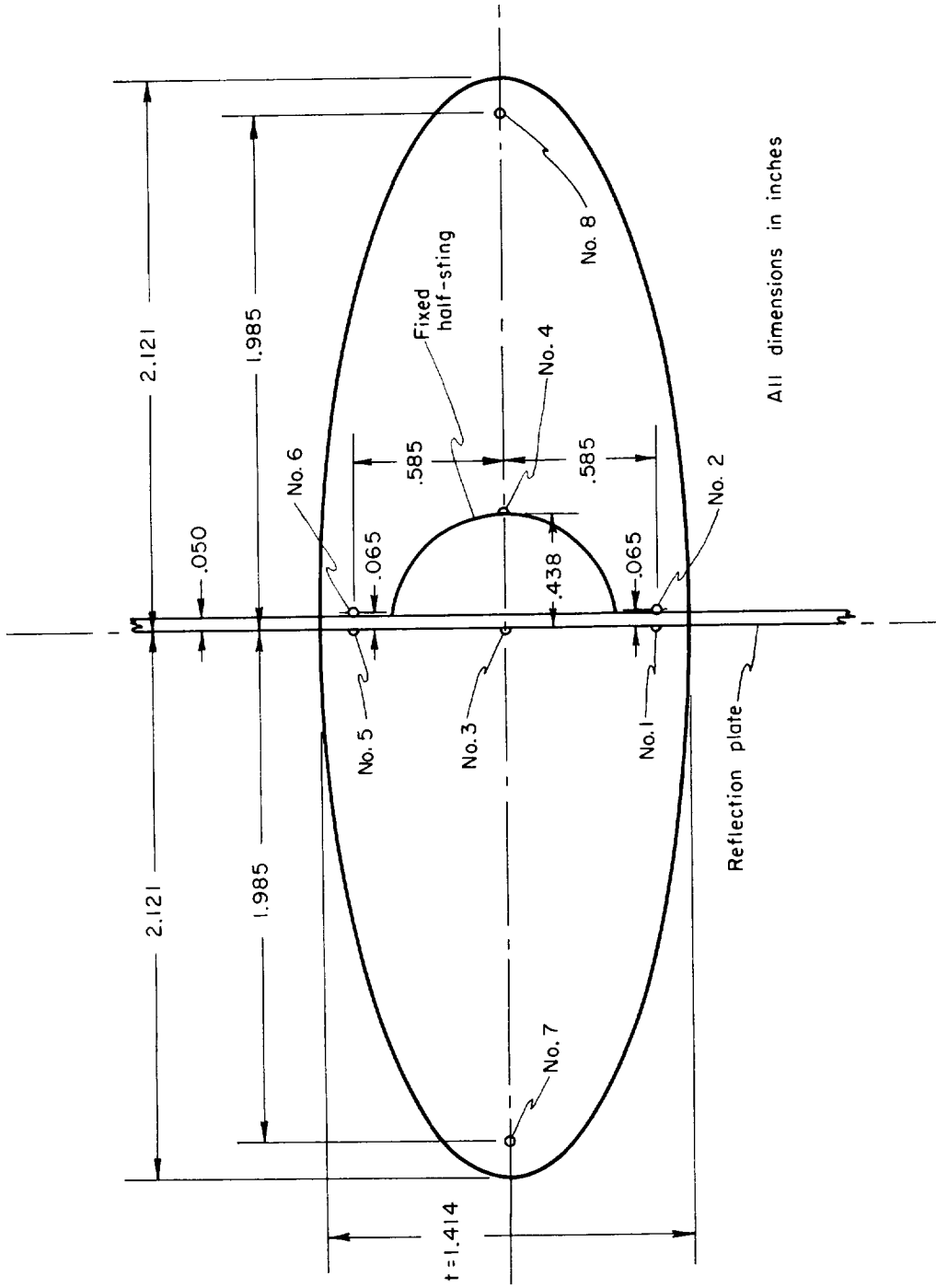
(c) Location and identification of base-pressure orifices.

Figure 1.- Concluded.
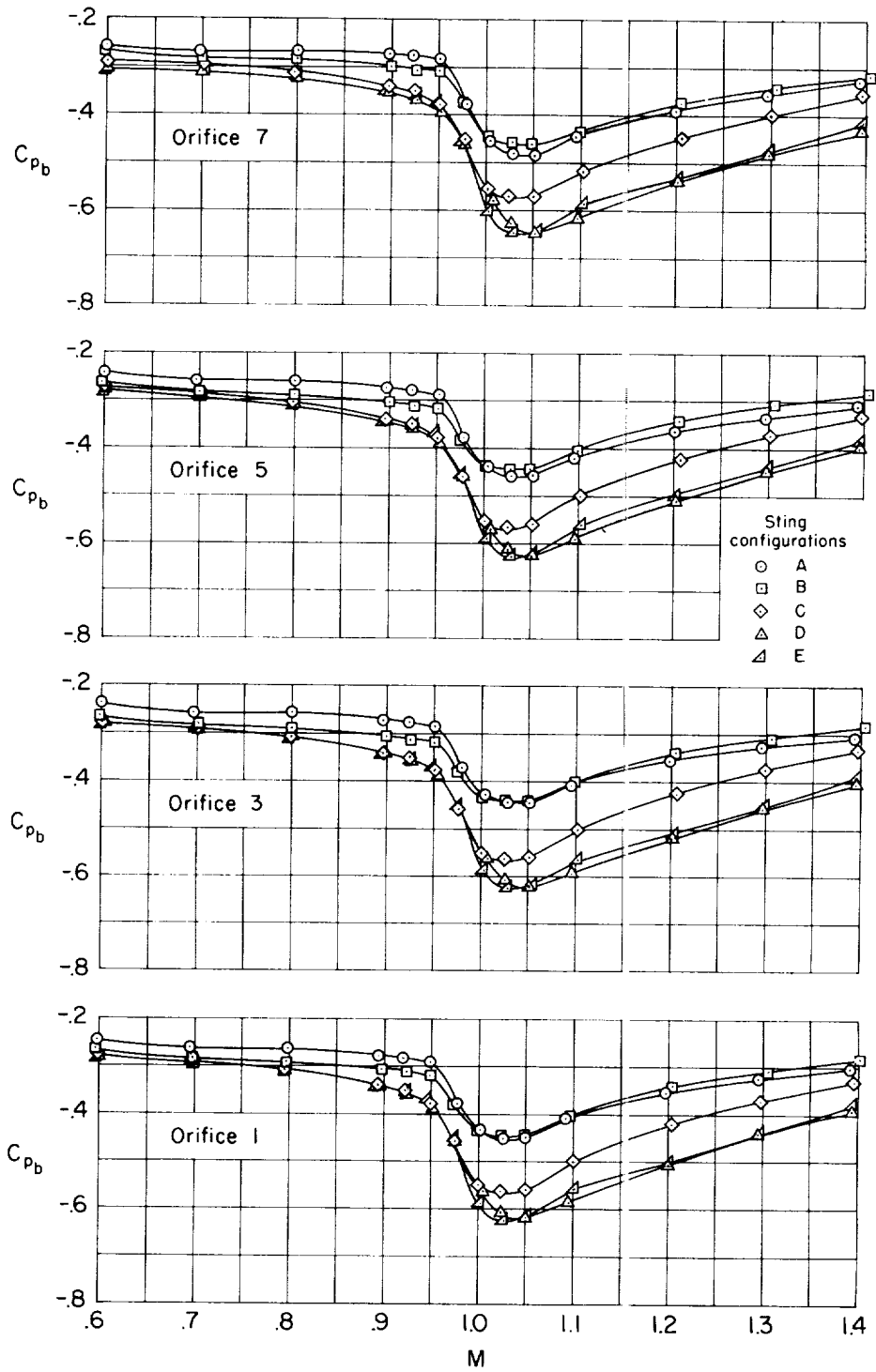
(a) $\alpha = 0^\circ$; removable sting side of reflection plate.

Figure 2.- Pressure coefficients for each orifice at the model base.
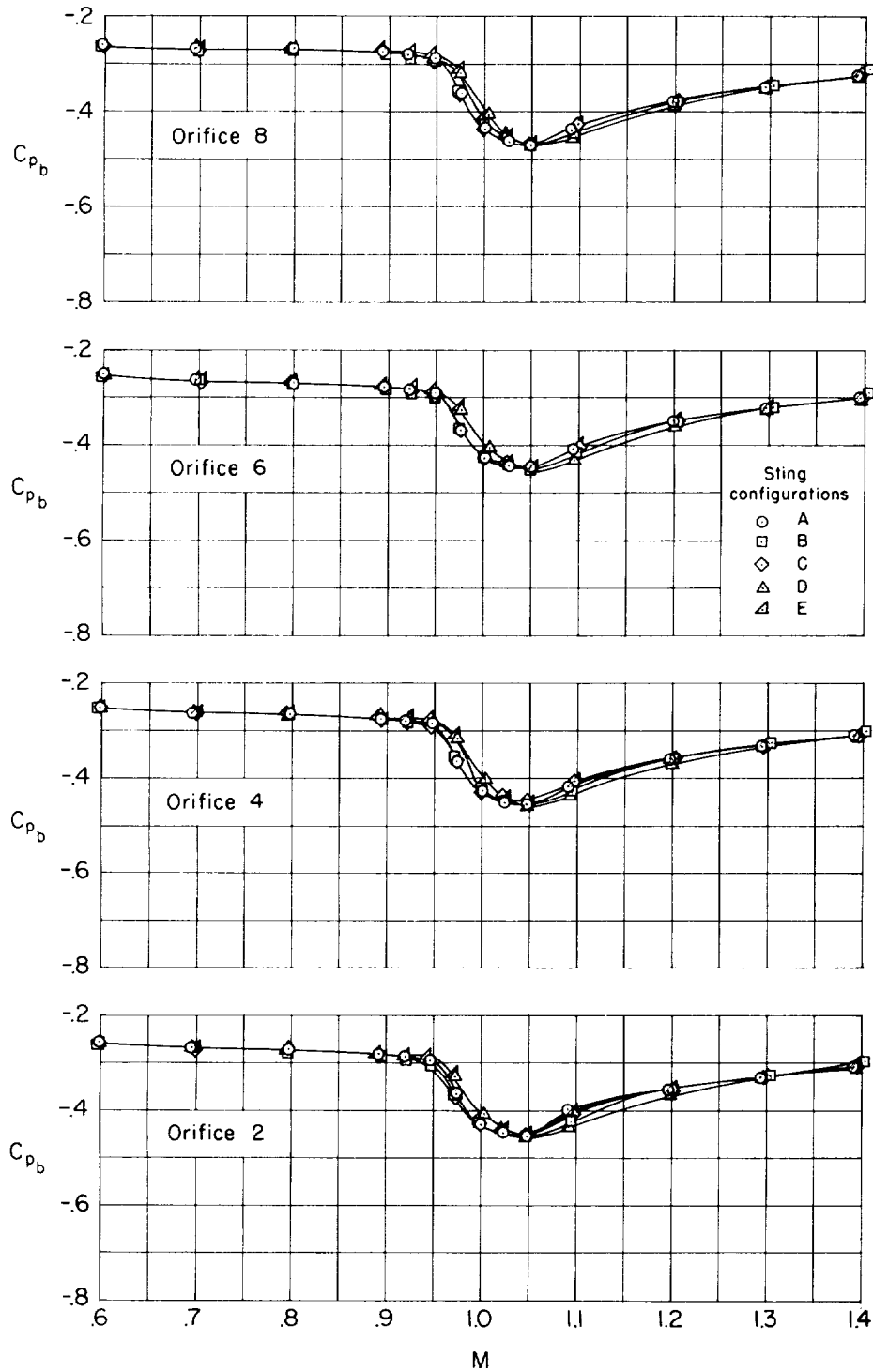
(b) $\alpha = 0^\circ$; fixed sting side of reflection plate.
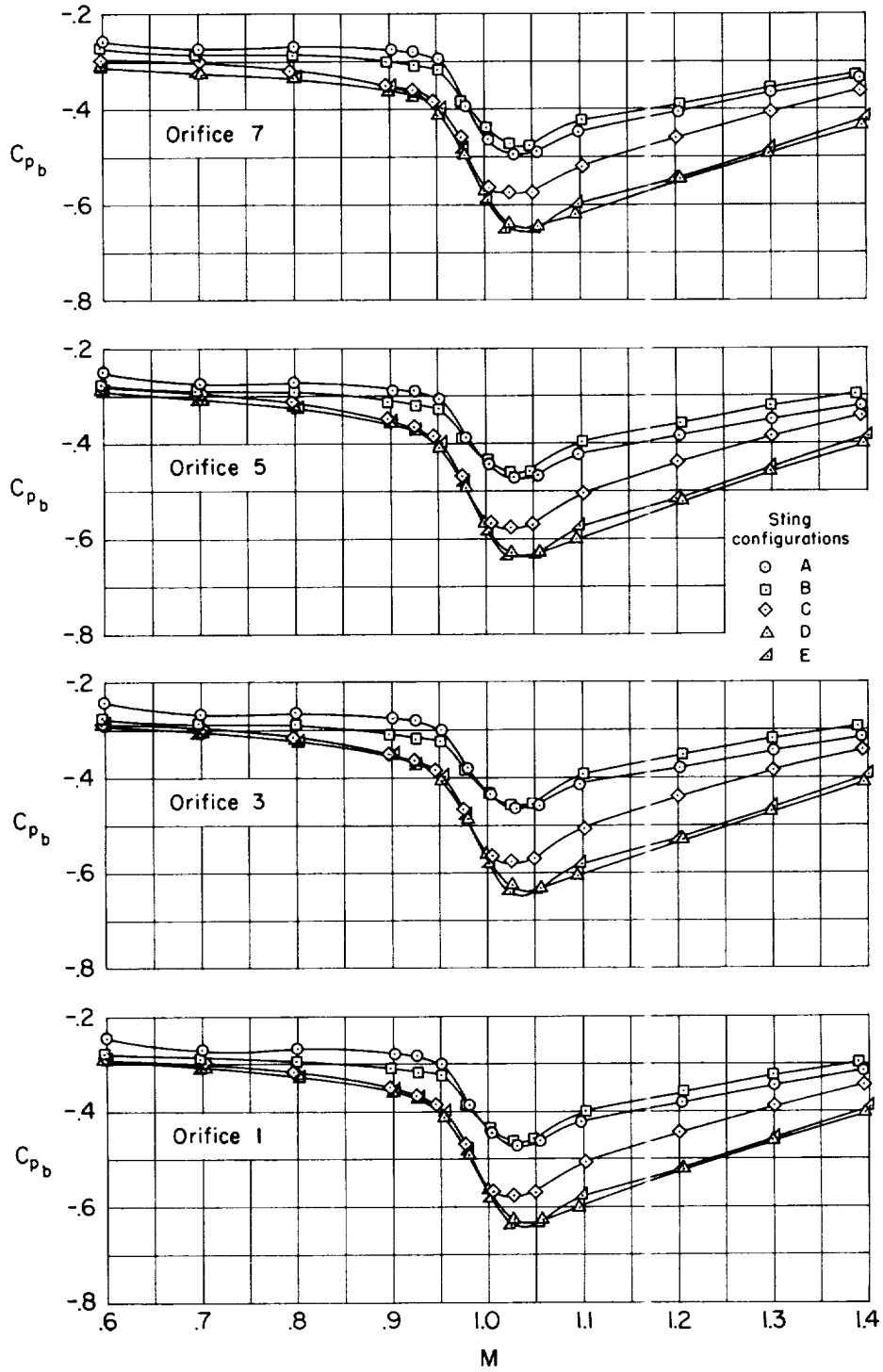
Figure 2.- Continued.

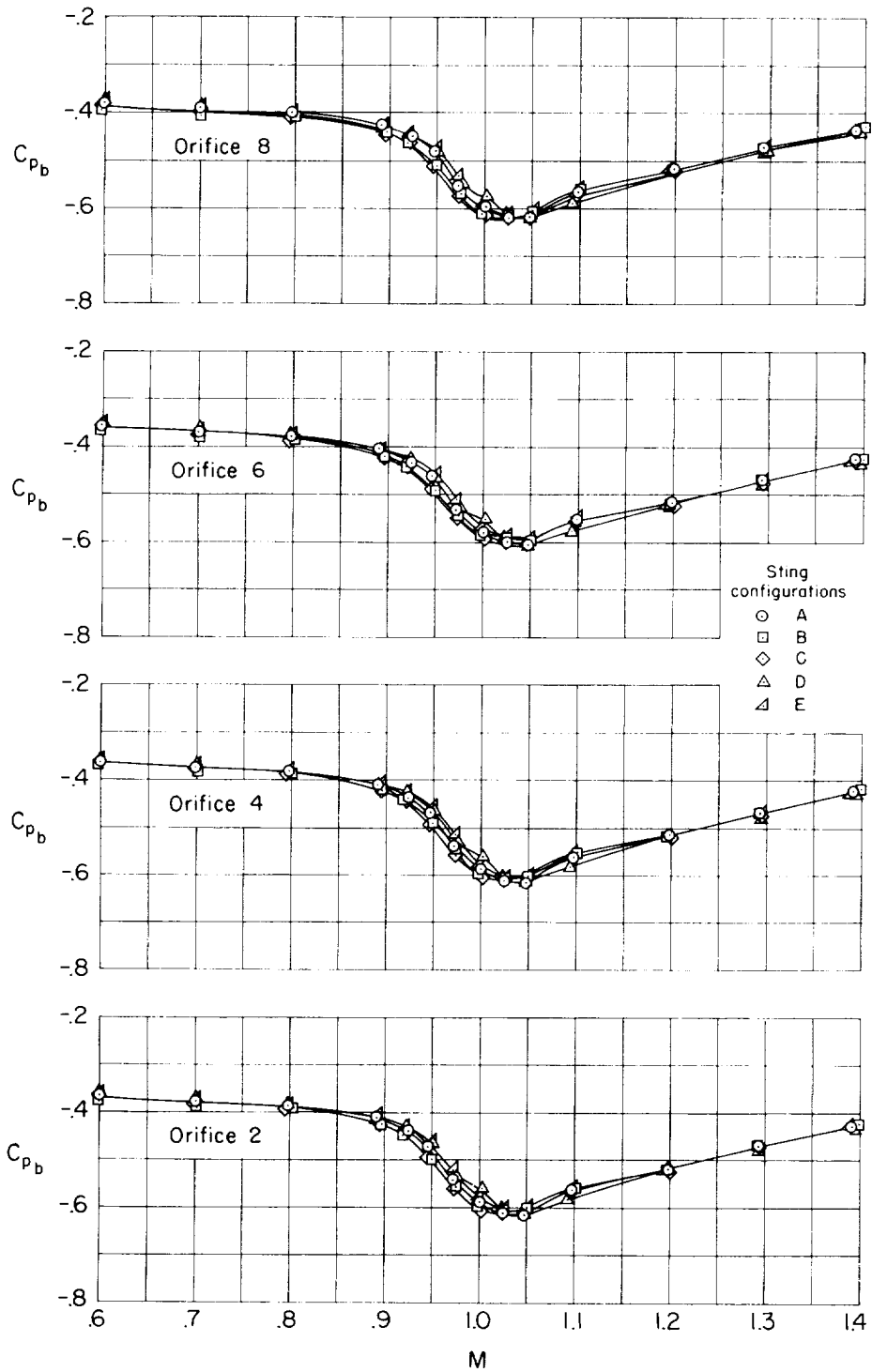(c) $\alpha = 4°$; removable sting side of reflection plate.
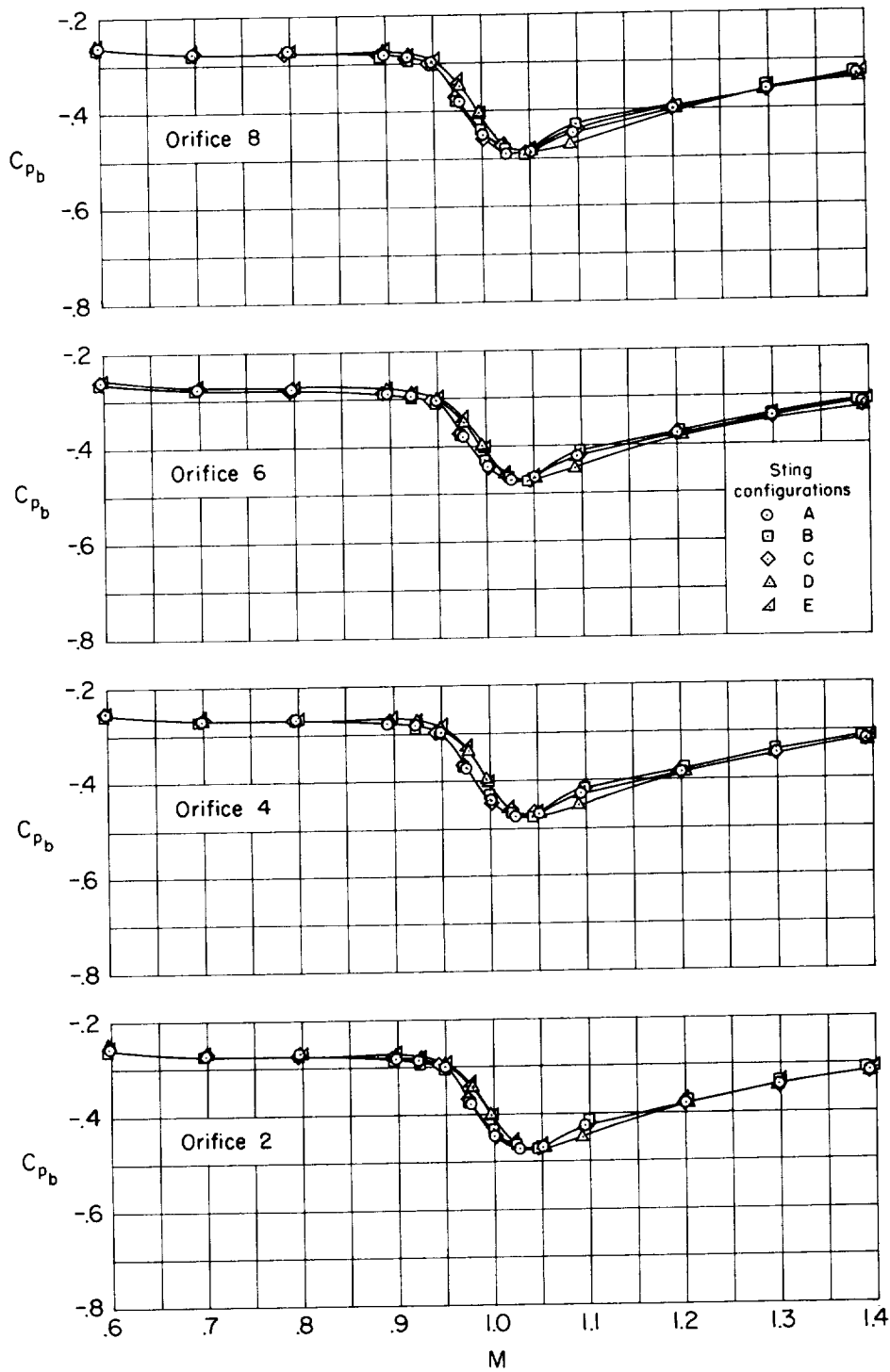
Figure 2.- Continued.
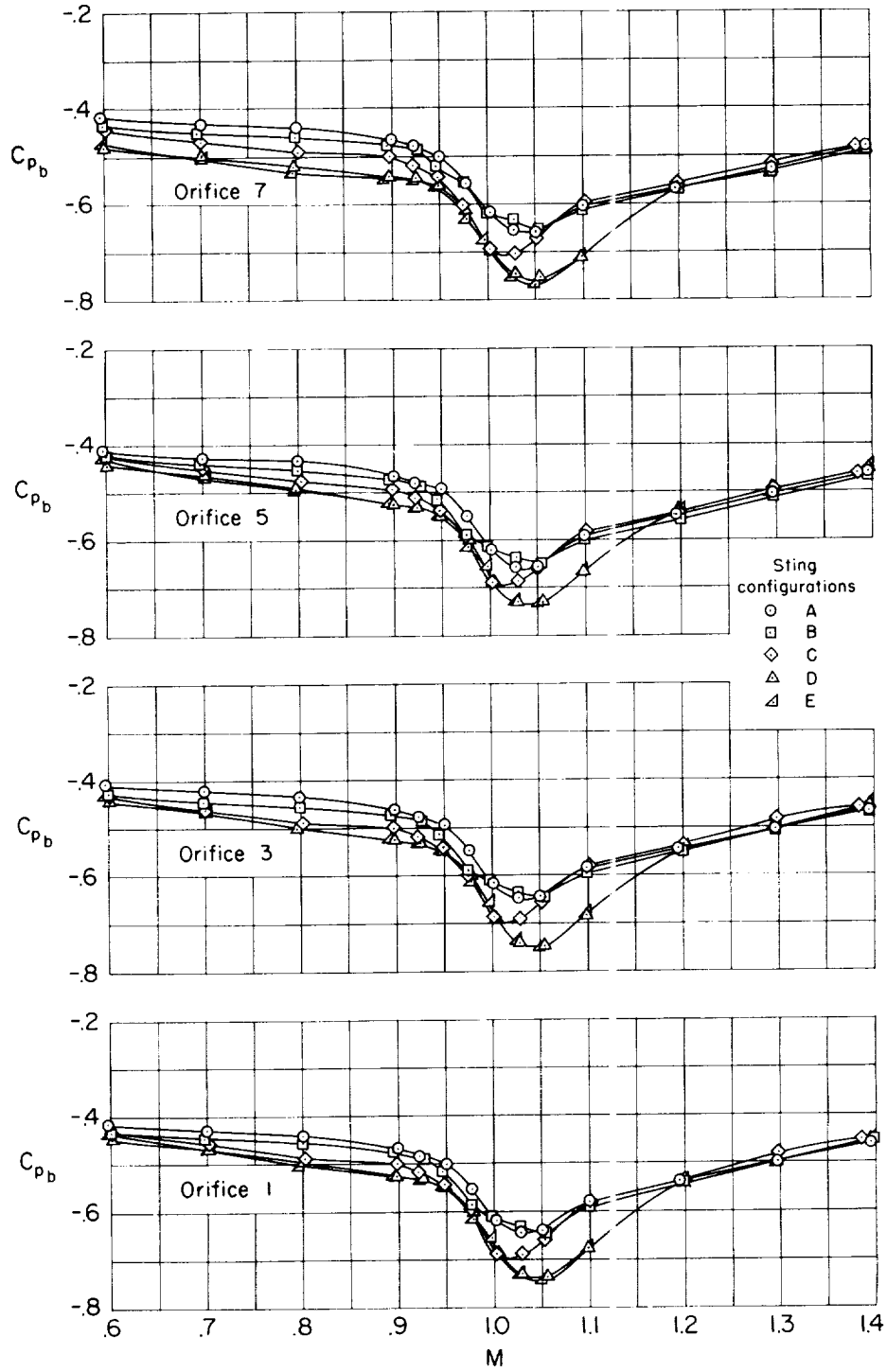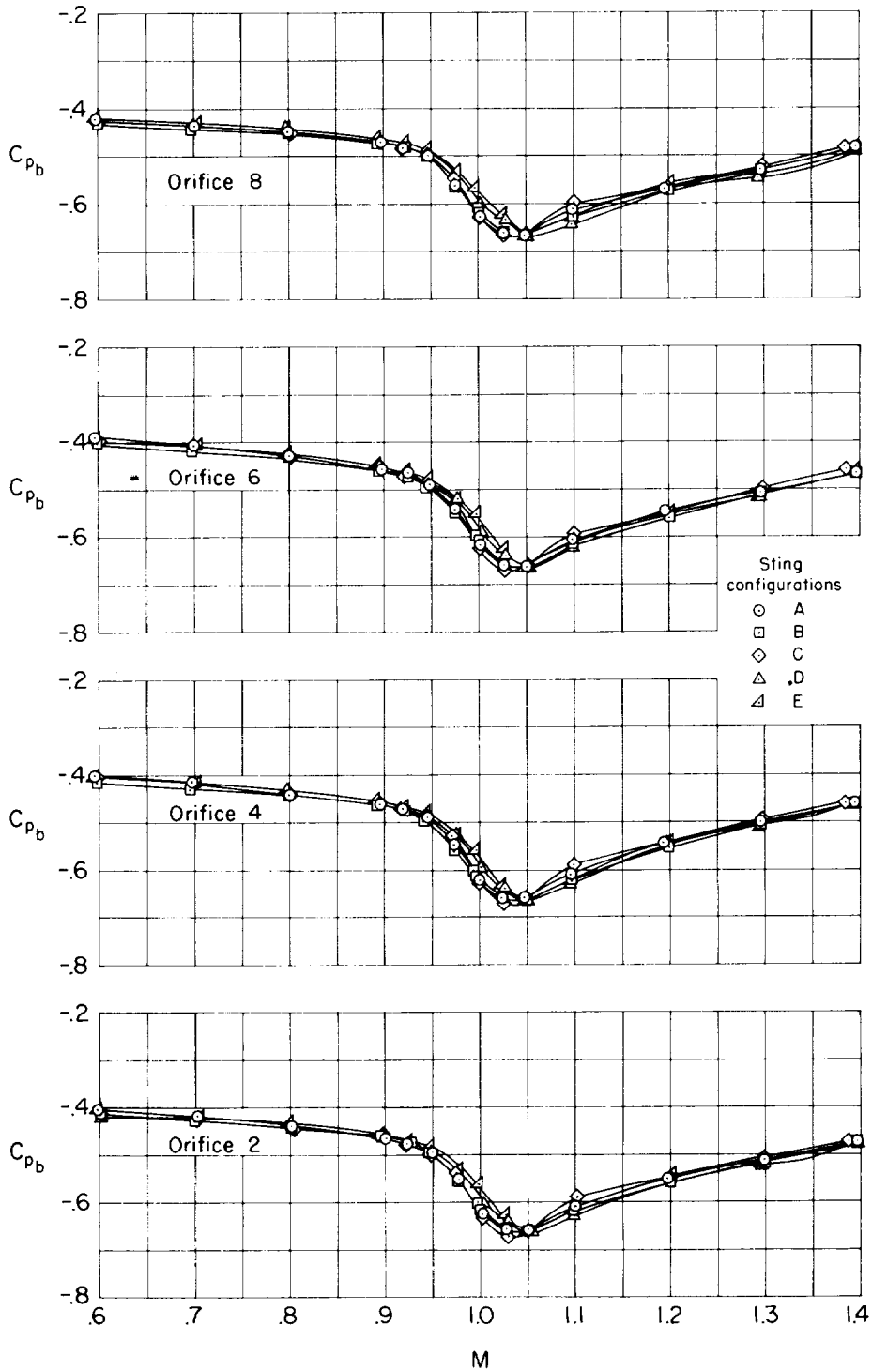
(d) $\alpha = 4°$; fixed sting side of reflection plate.
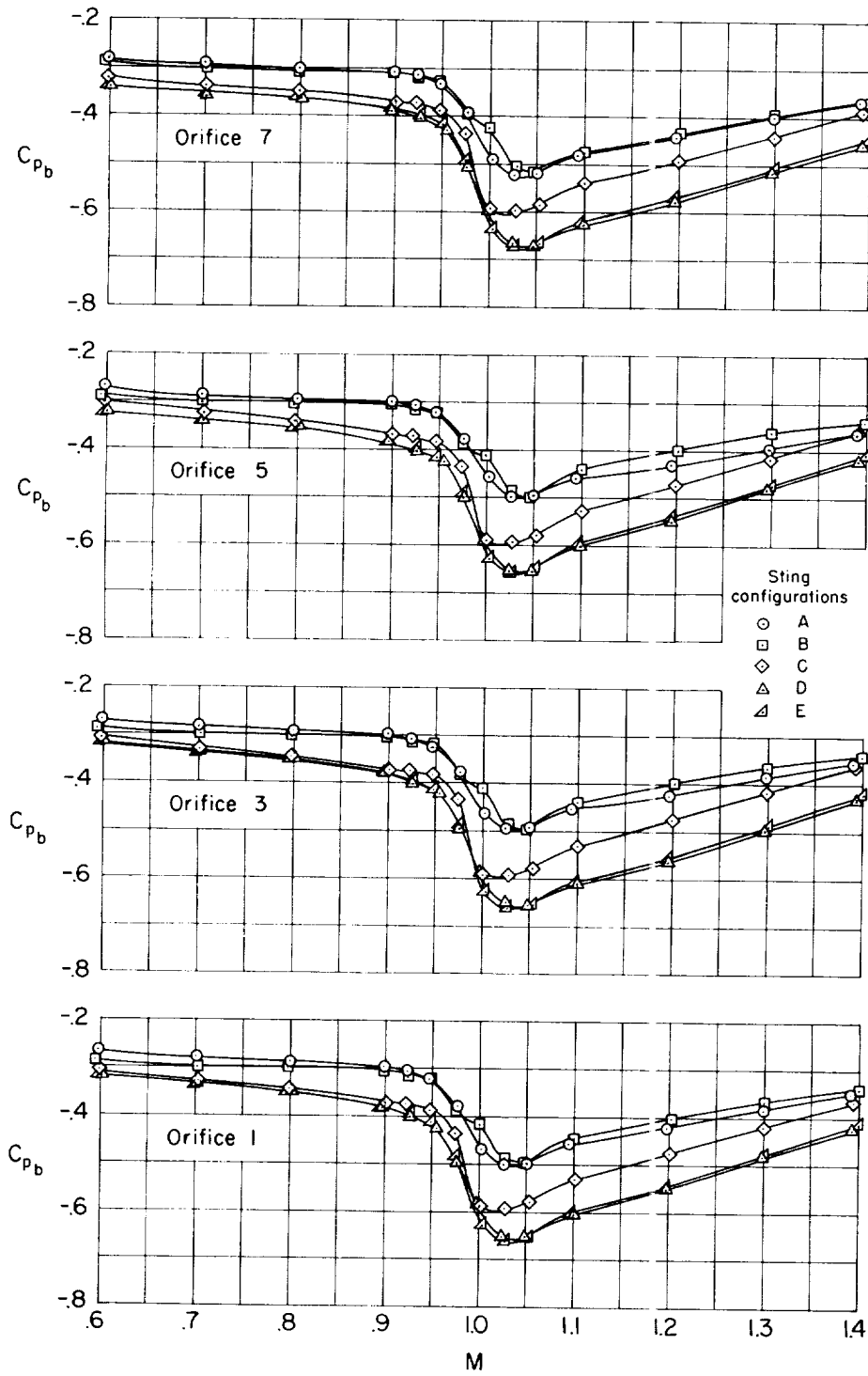
Figure 2.- Continued.

(e) $\alpha = 8°$; removable sting side of reflection plate.
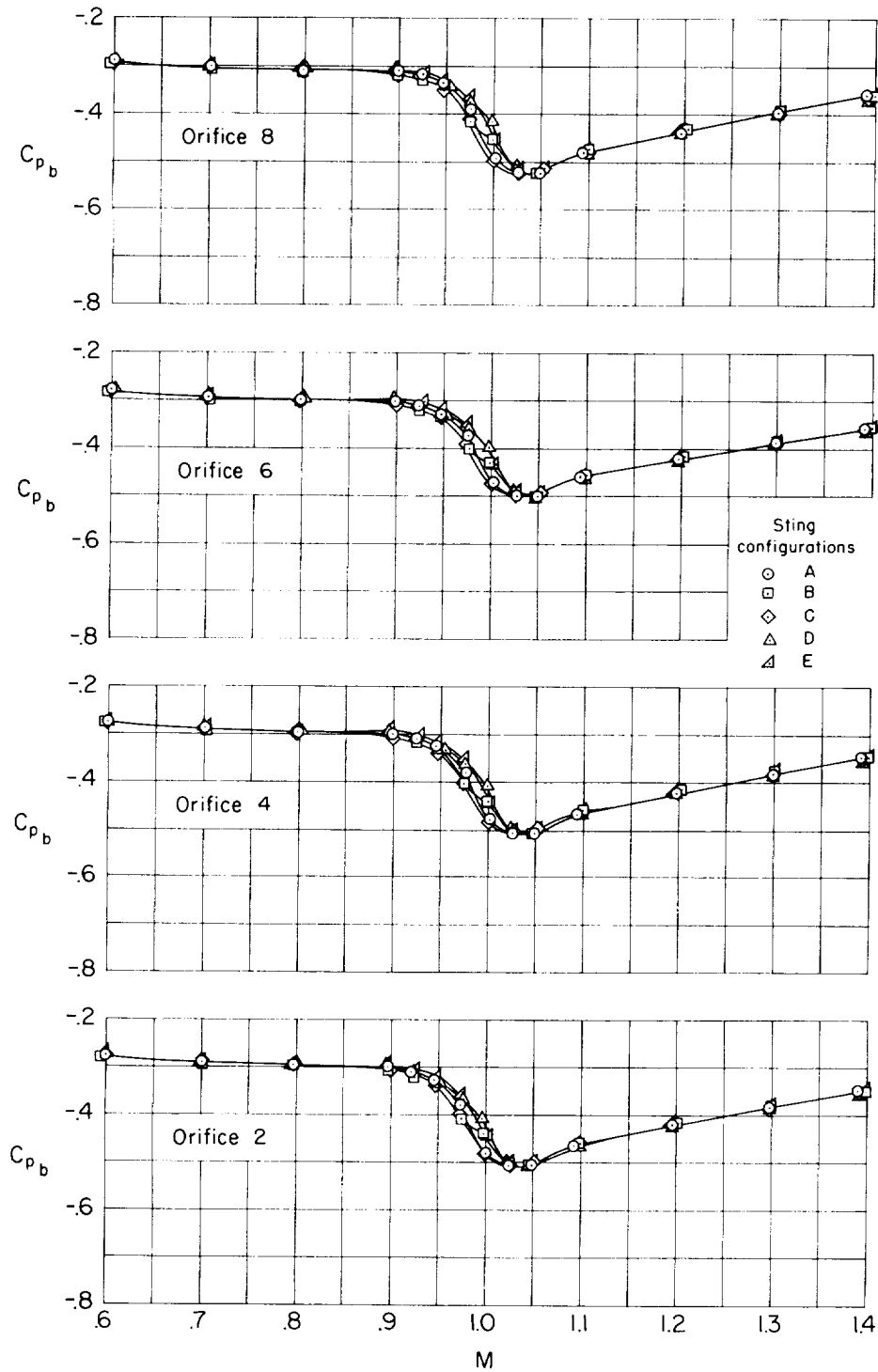
Figure 2.- Continued.

(f) $\alpha = 8^\circ$; fixed sting side of reflection plate.
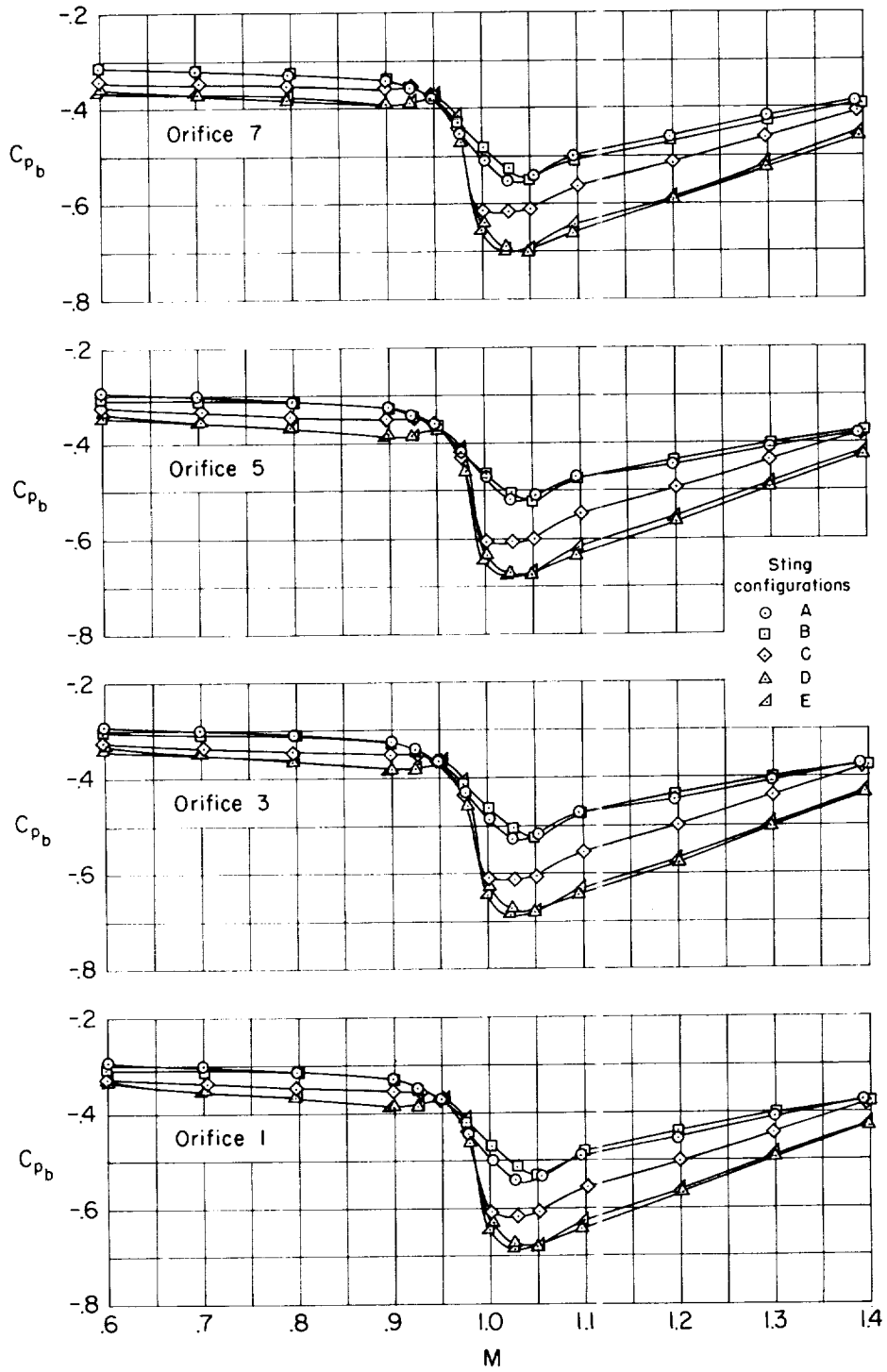
Figure 2.- Continued.

(g) $\alpha = 10^\circ$; removable sting side of reflection plate.
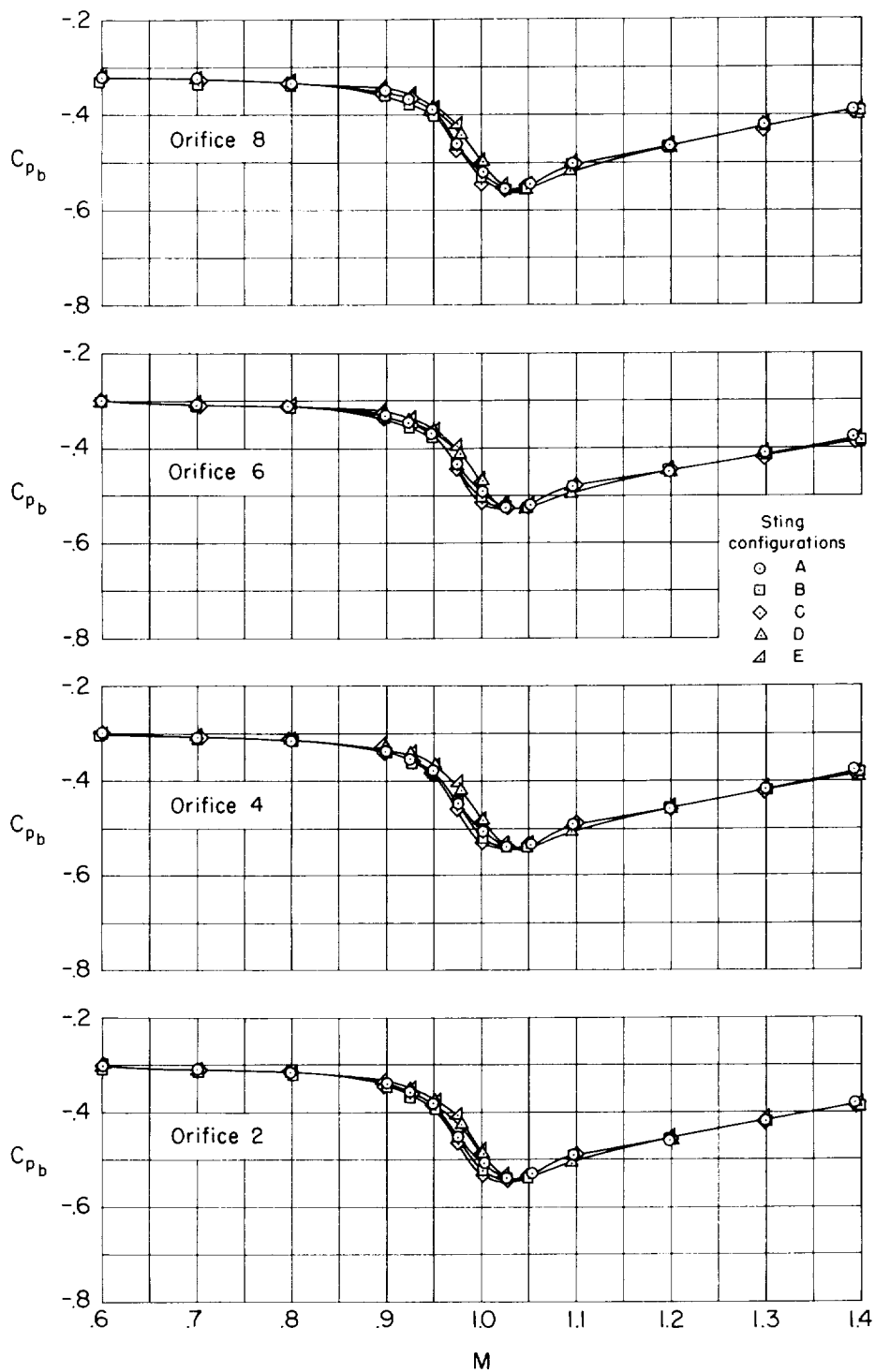
Figure 2.- Continued.

(h) $\alpha = 10^{\circ}$; fixed sting side of reflection plate.
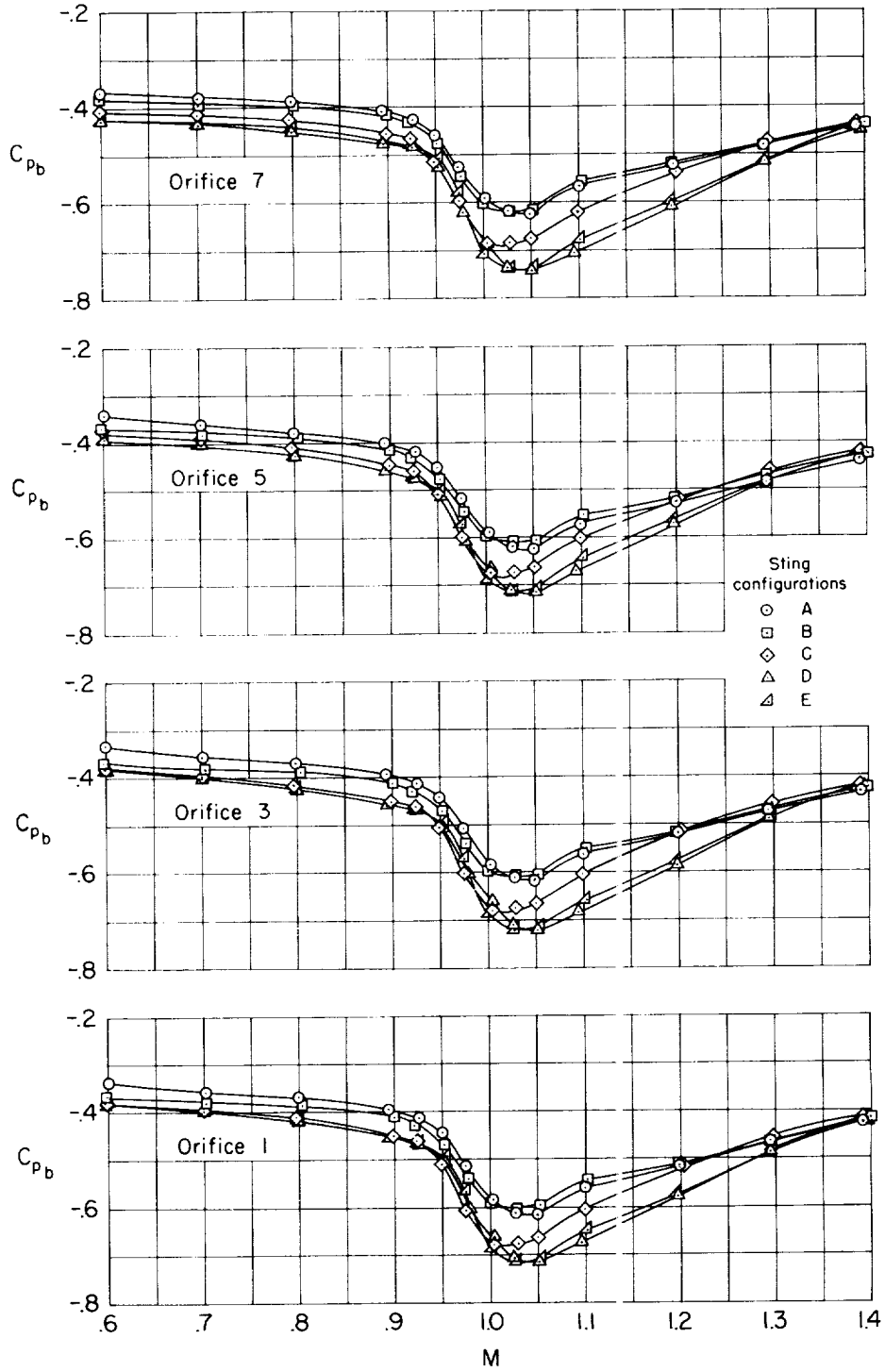
Figure 2.- Continued.

(i) $\alpha = 14^{\circ}$; removable sting side of reflection plate.

Figure 2.- Continued.

A
4
3
2

(j) $\alpha = 14°$; fixed sting side of reflection plate.

Figure 2.- Continued.

(k) $\alpha = 20°$; removable sting side cf reflection plate.

Figure 2.- Continued.

(l) $\alpha = 20°$; fixed sting side of reflection plate.

Figure 2.- Concluded.
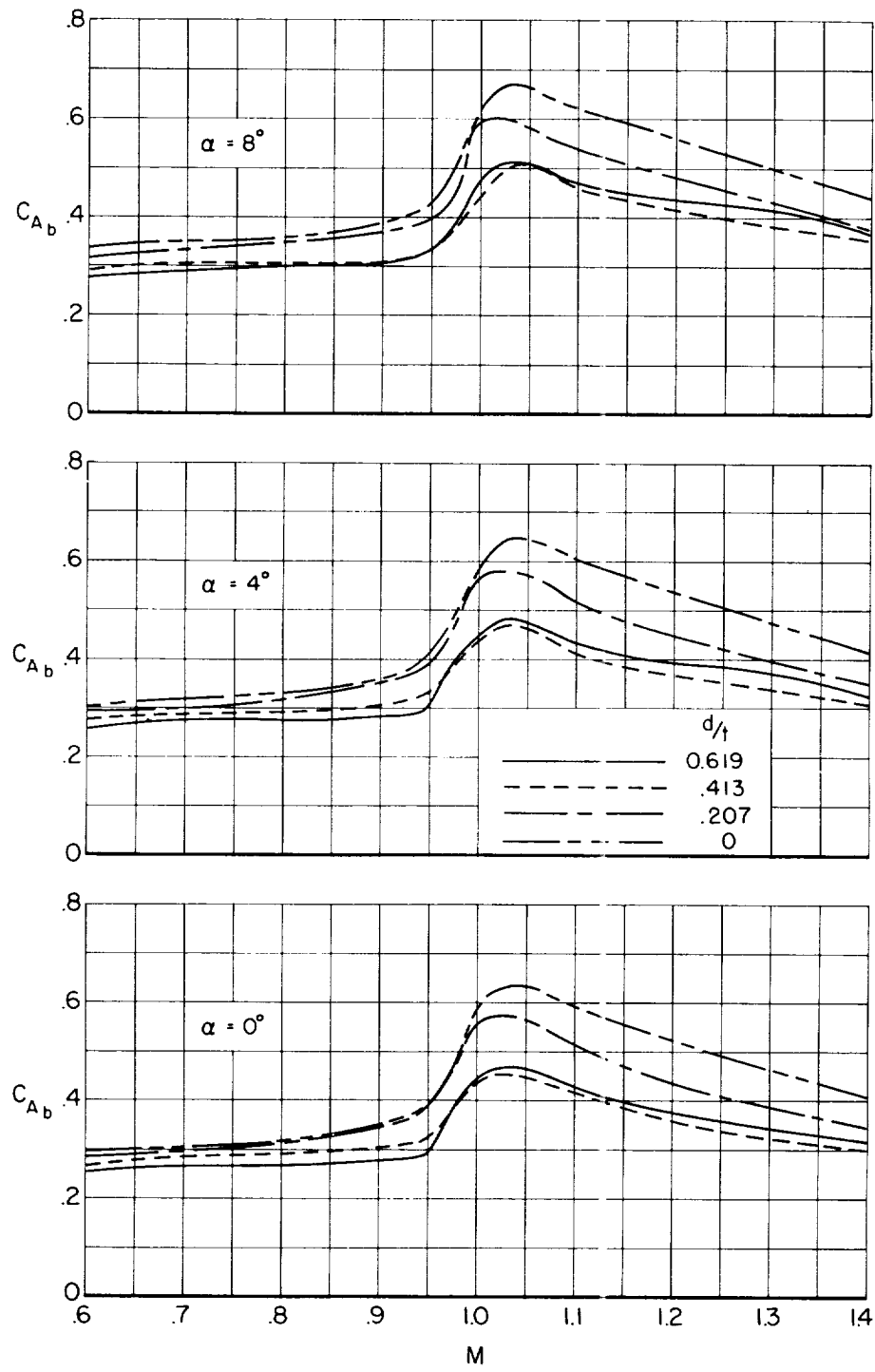
(a) Effects of Mach number on base axial-force coefficient;
$\alpha = 0^\circ$, 4°, and 8°.

Figure 3.- Base axial-force characteristics.
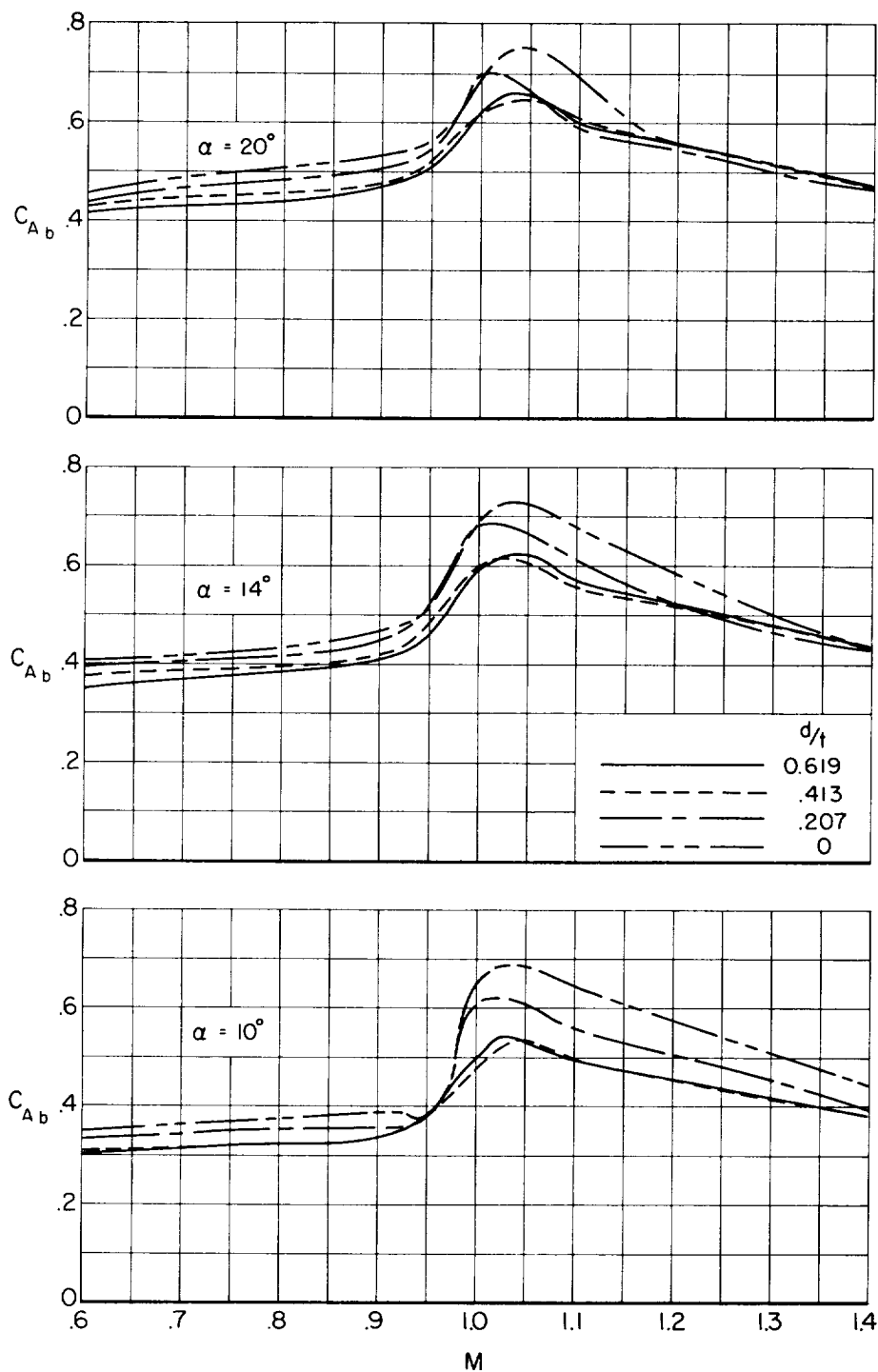
(b) Effects of Mach number on base axial-force coefficient;
$\alpha = 10^{\circ}$, 14°, and 20°.

Figure 3.- Concluded.
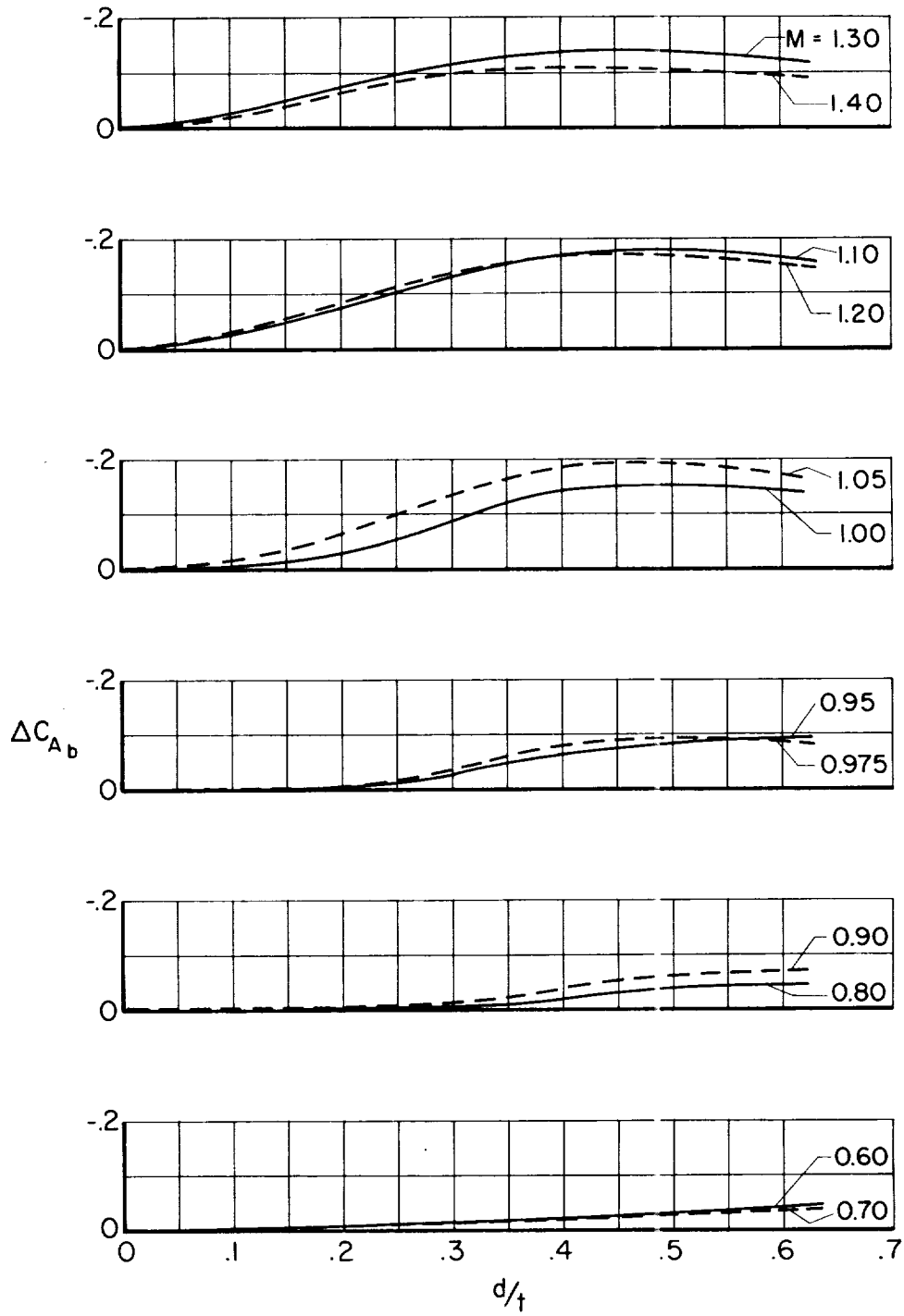
(a) $\alpha = 0°$.

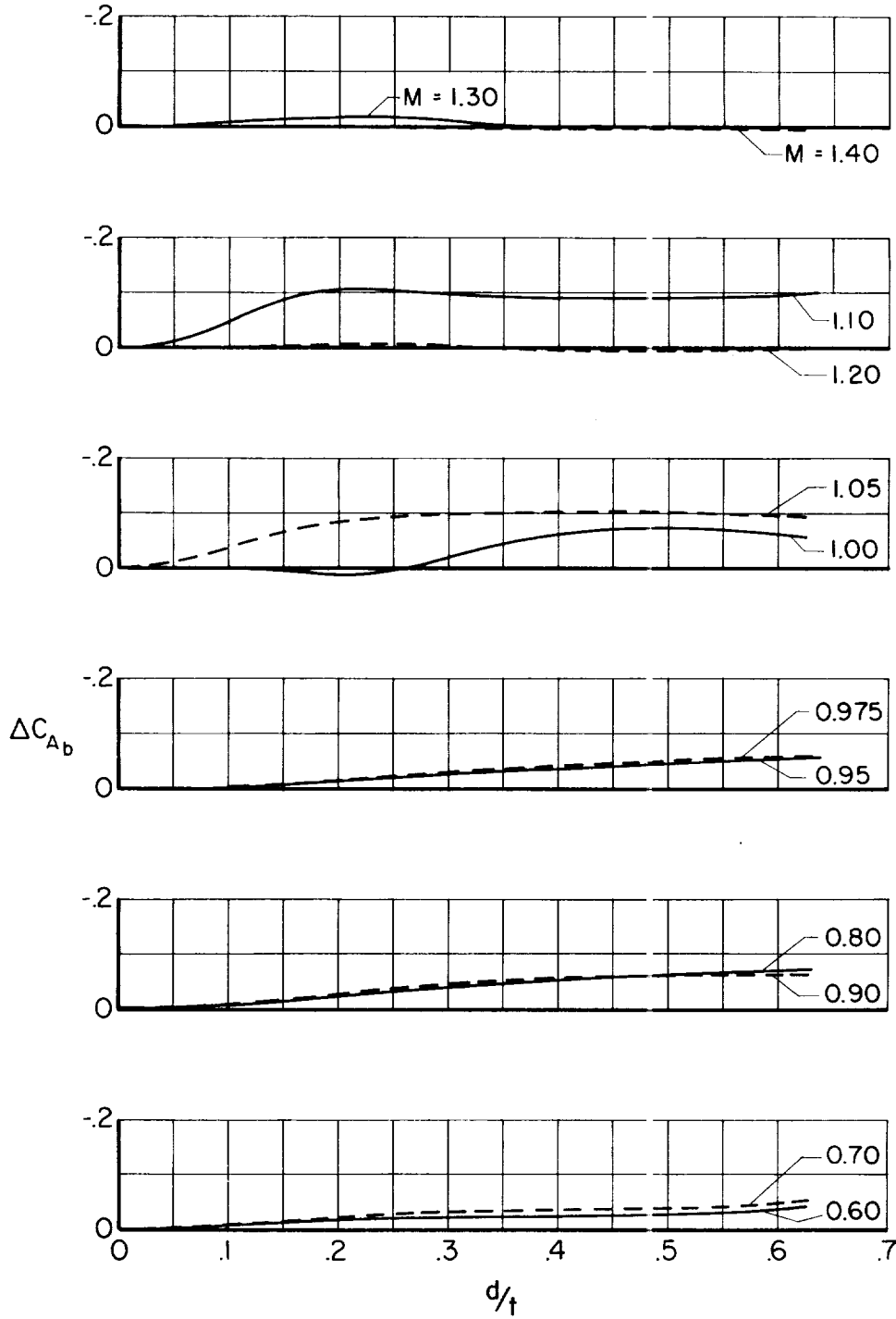Figure 4.- Effects of ratio of sting diameter to base thickness on the increments of base axial-force coefficient.
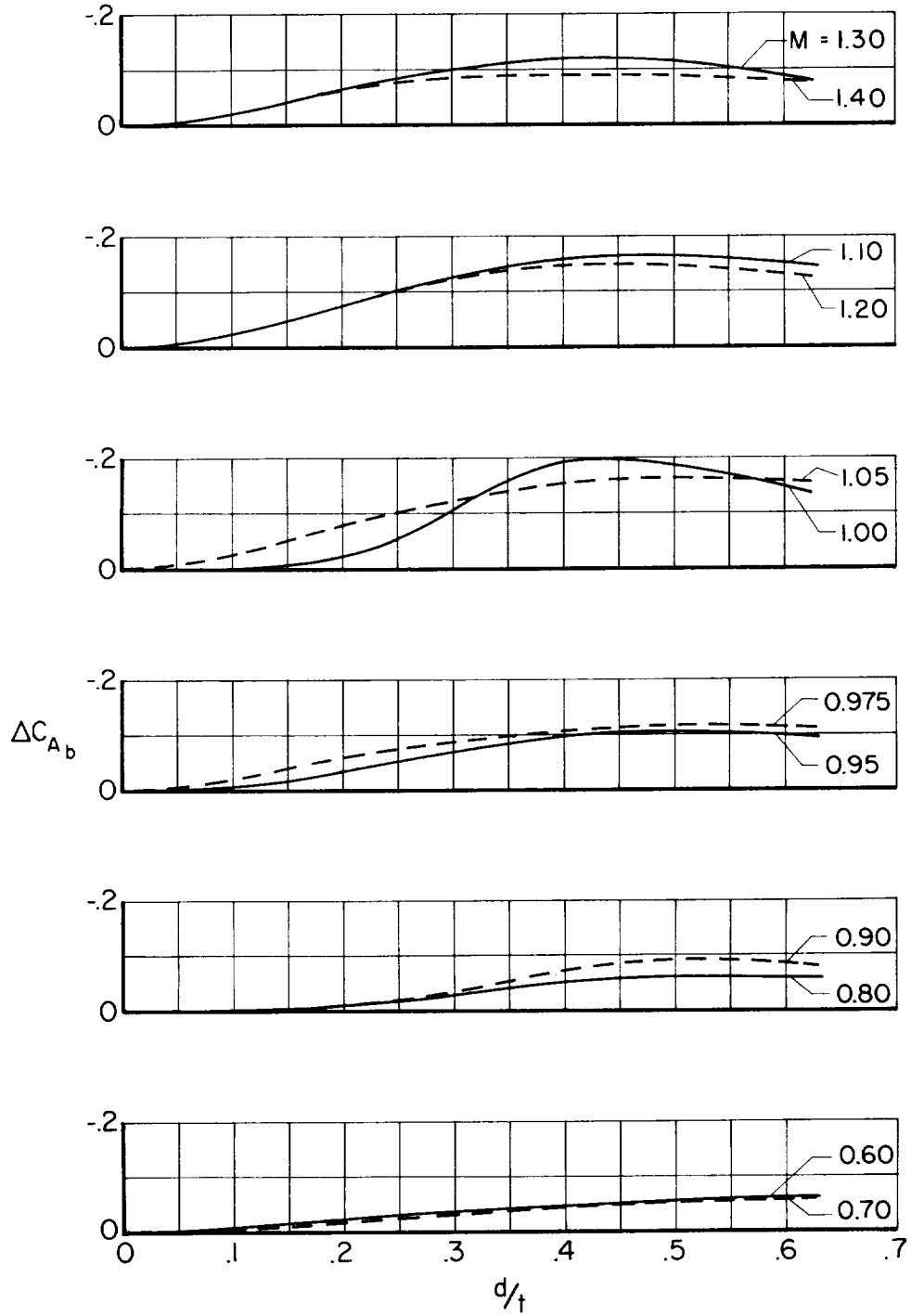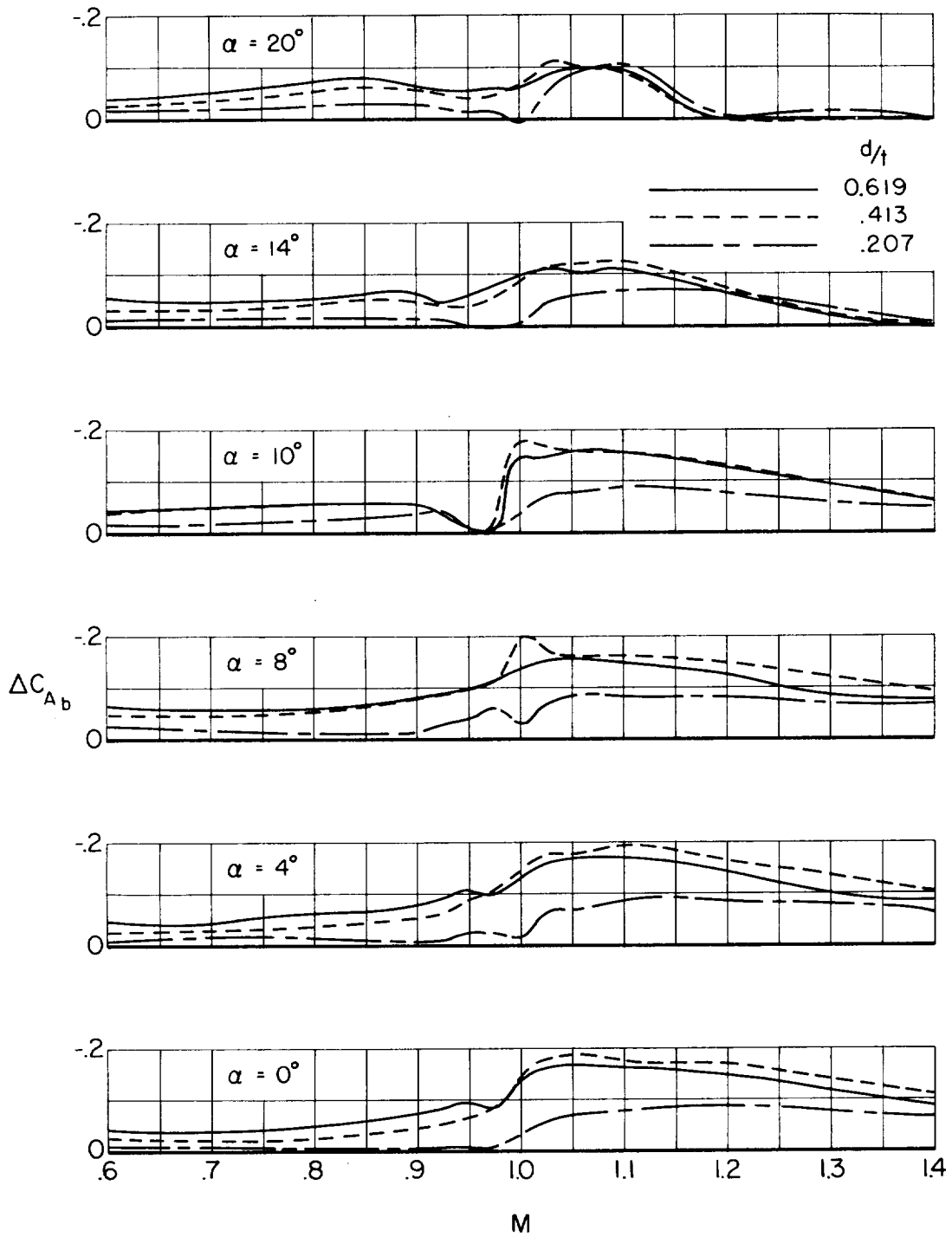
(b) $\alpha = 8^{\circ}$.

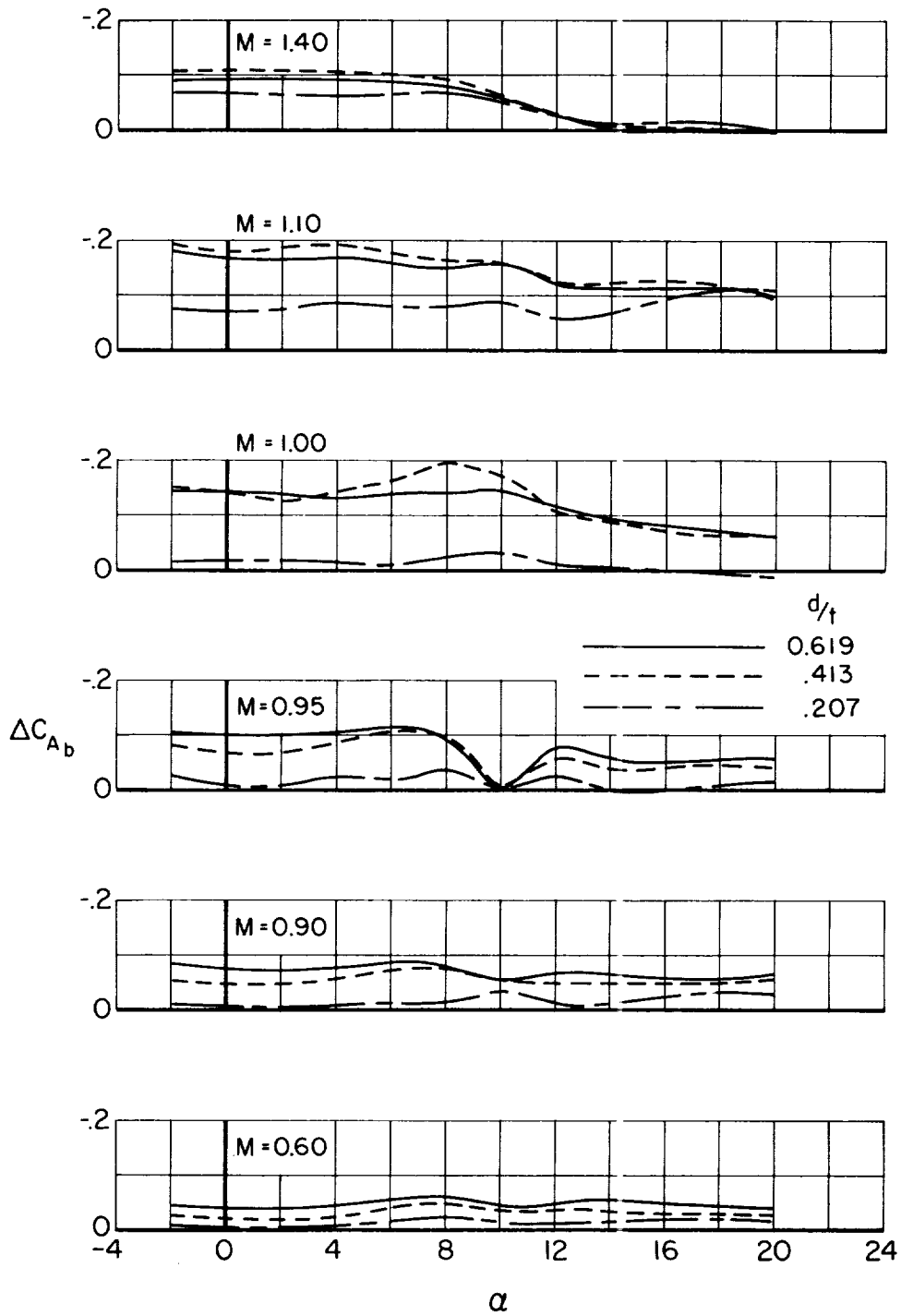Figure 4.- Continued.

(c) $\alpha = 20^\circ$.

Figure 4.- Concluded.

(a) Variations of ΔC_{A_b} with Mach number.

Figure 5.- Effects of Mach number and of angle of attack on the increments of base axial-force coefficient.

(b) Variations of ΔC_{A_b} with angle of attack.

Figure 5.- Concluded.